Hail storm hazard in urban areas: identification and probability of occurrence by using a single-polarization X-band weather radar

Vincenzo Capozzi[1], Errico Picciotti[2], Vincenzo Mazzarella[1], Giorgio Budillon[1], Frank Silvio Marzano[2,3]

[1] Department of Science and Technology, University of Naples "Parthenope", Centro Direzionale di Napoli, 80143, Italy
[2] Centre of Excellence CETEMPS, University of L'Aquila, 67100, Italy
[3] Dept. of Information Engineering, Sapienza University of Rome, 00184, Italy

Correspondence to: V. Capozzi (vincenzo.capozzi@uniparthenope.it)

Abstract. This work exploits the potentiality of hail warning, based on single-polarization X-band weather radar measurements and tested on a large and well-documented data set of thunderstorm events in southern Italy near Naples. Even though X-band radars may suffer of two-way path attenuation especially at long ranges, due to their relatively low cost their use is rapidly increasing for short-range applications such as urban environments. To identify hail through radar measurements, two different methodologies have been selected and adapted to X-band data within the study area: one uses the Waldvogel (WAL) approach, whereas the other one uses the Vertically-Integrated Liquid Density (VIL-Density) product. The study aims at developing a Probability-of-Hail (POH) index in order to support hail risk management at urban scales. In order to find the optimal threshold values to discriminate between hail and severe rain, an extensive intercomparison between outcomes of the two methodologies and ground truth observations of hail has been performed, using a 2x2 contingency table and statistical scores.

The results show that both methods are accurate for hail detection in the area of interest, although VIL-Density product is less satisfactory than WAL method in terms of false alarm ratio. The relationship between the output of these two methodologies and POH has been derived through a heuristic approach, using a third-order polynomial fitting curve. As an example, the POH indexes have been applied for the thunderstorm event occurred on 21 July 2014, proving to be reliable for hail core detection.

1 Introduction

In recent years, urban areas have experienced a strong vulnerability to severe convective events, such as torrential rainfall, hail, lightning, wind storms and convective outbreaks (Marzano et al., 2012). The increased exposure to meteorological hazards is due both to the climate change, which has altered the temporal and spatial patterns of precipitation, and to the diffusion of complex networks infrastructures. Because of the high cost associated with severe weather occurrence, the need in urban areas of reliable monitoring and nowcasting techniques of weather hazards has recently increased. Nowdays, most of those techniques are based on weather radars, because the latter are capable to monitor precipitation at a resolution and areal extent previously impossible with rain gauge networks. The use of weather radar in urban hydrology is mainly focused on the development of high-resolution rainfall estimates, which serve as input for the modeling of urban drainage systems (e.g. Tilford et al., 2002).

In this work, we explore the usefulness of meteorological radar in urban environment for the real time detection of hail precipitation, which is one of the most widespread and damaging convective hazard. Hail events cannot be easily monitored using ground observational networks, due to their high variability in time and space. The only instrument that is able to measure hail size and kinetic energy distributions is the disdrometer (a sensor that measures particle size distribution). However, the high costs and fragile nature of this instrument prohibit the growth of a dense network of stations. Therefore, as stated in Kunkel et al. (2013), hail (and all severe convective hazards, including tornadoes and thunderstorm winds) was considered in the lowest category of detection knowledge. The majority of the available information on hail and its frequency has come from hail storm reports provided by volunteers. Those reports have the drawback of being subjected to large spatial and reporting biases resulting from population density.

For the reasons stated above, weather radars appear as a valuable instrument for the real time observation of hail. In addition, volumetric radar data allow estimating the vertical extension of thunderstorm cells. The latter information is very useful for hail detection purpose, since the severity of thunderstorm is strongly related to its vertical extension (Delobbe et al., 2003).

Nowadays, the methodologies based on dual polarization weather radar are the most used to distinguish between rain and hail (e.g. Aydin et al., 1986; Straka et al., 2000; Marzano et al., 2007), because they are able to provide a direct distinction between the rain droplets and the hailstones. As well as measuring the standard horizontally-polarized reflectivity (Z_H), a dual polarization weather radar also measures the ratio of the reflected horizontal and vertical power returns (Z_V). This ratio, called ZDR (differential reflectivity), usually in pure rain is positive (especially for heavy rain) whereas in hail its value is near zero (the latter tends to tumble randomly and thus, to the radar, appears to be spherical).

Single-polarization weather radars cannot distinguish among different types of hydrometeors. However, some features in the vertical profile of reflectivity, including high reflectivities occurrences above specific environmental temperature heights, can represent the physical processes related to the hail growth (Skripniková and Řezáčová, 2014). Several methodologies for the identification of hail events from single-polarization weather radar measurements have been proposed in the available literature (Holleman, 2001). Some methods use threshold values for a hail-related quantity, such as reflectivity in low-level CAPPI (Geotis, 1963), vertically-integrated liquid density (Amburn and Wolf, 1997) or the difference in altitude between the height of zero-degree isotherm and the highest level attained by 45-dBZ reflectivity core (Waldvogel et al., 1979). Other methods transform radar-based products into probability values, such as the Hail Detection Algorithm (Witt et al., 1998) and the Probability of Hail (Delobbe and Holleman, 2006). Several algorithms combine radar measurements with other meteorological data; for example, aerological data are used in Waldvogel et al. (1979) and in Witt et al. (1998). Auer (1994) proposed a technique that matches radar reflectivity measurements with satellite-derived cloud top temperatures. Various hail identification techniques for Ebro valley region in Spain have been considered in Mallafre et al. (2009): among these, the one based on kinetic energy flux was found to be the best for distinguish between hail and no-hail precipitation in the studied area.

However, the charges of installation and maintenance of conventional weather radars, such as S-band and C-band systems, constitute one of the major limitation for their widespread diffusion. A good and reliable alternative is represented by low-cost short-range X-band radar systems. Although the latter suffer strongly from beam attenuation along the path, especially

in convective rain events and at long ranges, they have the advantage of performances comparable with conventional systems, but typically with smaller antenna and lower power consumption (Van de Beck et al., 2010). The impact of two-way path attenuation at X band is reduced if these low-cost radars are used at short ranges, as for urban area monitoring. In recent years, the increasingly use of X-band weather radars, both in single and in dual polarization mode, encouraged the development of systematic approaches to mitigate their limitations and to enhance their promising potential in severe weather surveillance at short ranges (e.g. Anagnostou et al., 2004; Matrosov et al., 2005; Montopoli et al., 2010; Marzano et al., 2010; Van de Beek et al., 2010; Marzano et al. 2012).

Since November 2011, a single-polarization X-band weather radar, called WR-10X, has been installed in Naples' urban area at the top of Castel Sant'Elmo (40.8438°N, 14.2385°E, 280 m asl). The radar belongs to the Campania Center for Marine and Atmospheric Monitoring and Modelling (CCMMMA) of University of Naples "Parthenope". First studies have been devoted to quality control and correction of radar data, to improve WR-10X quantitative precipitation estimates with a raingauge-based adjustment method (Capozzi et al., 2014) and to generate a preliminary hail detection product based on vertically-integrated liquid density method (Marzano et al., 2012; Capozzi et al., 2015).

The aim of this work is to develop a probability of hail occurrence algorithm, based on WR-10X measurements, that could be particularly useful to mitigate hail-induced risks in Naples urban area. In order to achieve the goal of this study, two hail detection methods were applied and adapted: the Waldvogel criterion (WAL) (Waldvogel et al., 1979) and the Vertically-Integrated Liquid Density (VIL-Density) technique (Amburn and Wolf, 1997). The first one combines radar reflectivity data with other sources of information (sounding data or meteorological in situ data), whereas the VIL-Density product is derived exclusively from radar scans. Both methods have been selected and adapted to X-band after considering their easy exploitation for an operational use.

The originality of this paper, with respect to previous studies devoted to the development of a radar-based hail detection product, lies in the two following aspects:

1. For the first time, using a large dataset of thunderstorm events, a single-polarization X-band miniradar has been used to generate an innovative experimental probability of hail index valid for an urban area. Therefore, the advantages introduced by X-band systems in terms of better spatial and temporal resolution than conventional weather radars are fully exploited. The prototype radar system tested in this study constitutes one of the challenges in the near future radar meteorology, because it combines a relatively high quality of measurements with affordable cost of infrastructure.

2. With respect to the first preliminary studies (Marzano et al., 2012; Capozzi et al., 2015) performed about the topic addressed in this paper, a technique that matches radar reflectivity data with other sources of meteorological information, i.e. the WAL method, has been used to generate a probability of hail index. Therefore, the potential advantages introduced by the combination between single-polarization X-band miniradar measurements and

conventional meteorological data are for the first time explored. In addition, we optimize the performance of WAL method in relation to the study area and to X-band miniradar tested in this work, by proposing a variant of the original criterion developed by Waldvogel et al. (1979).

The two different algorithms (WAL and VIL-Density) have been compared and verified for 53 thunderstorm events observed in Campania Region between April 2012 and June 2015. Days with thunderstorm occurrence in the examined period have been identified means of Synop stations, while hail reports have been provided by weather amateurs and newspapers. The evaluation of the two hail detection techniques is based on a number of verification scores (probability of detection, false alarm ratio, critical success index and probability of hail), that are calculated from contingency table.

The hail detection product developed in this work could be of high interest in the context of operational meteorology. Although it was developed for a specific area (i.e. Naples metropolitan environment), it can be easily adapted to other specific areas where detailed meteorological information is needed for a solid severe weather surveillance system.

This paper is organized as follows. In section 2, the two selected algorithms for hail detection are described. The third section provides information about radar data processing and a description of the study area; this section also addresses the hail events examined. The verification scores used in statistical analysis and the results of the study are presented in the fourth section. Finally, the capabilities of the two criteria are applied to a summer hail event occurred in July 2014.

2 Hail detection radar algorithms

The two hail detection algorithms are here illustrated and their adaptation to Naples X-band single-polarization radar measurements discussed.

2.1 Waldvogel method

The WAL technique relies on the difference (ΔH), in (km), between the maximum altitude attained by a determined reflectivity core (H_{Zt}) and the zero-degree isotherm height (H_{T0}) (Fig. 1).

$$\Delta H = H_{Zt} - H_{T0} \quad (1)$$

In the original criterion defined by Waldvogel et al. (1979), Eq. (1) has been computed using the 45-dBZ reflectivity core. The occurrence of hail is likely if:

$$H_{Z45} \geq H_{T0} + 1.4 \text{ km} \quad (2)$$

As highlighted from Fig. 2, the probability of hail rises as the altitude of 45-dBZ reflectivity core increases above the zero-degree isotherm level. In order to detect hail, this technique considers two elements involved in the hail formation process: the occurrence of a remarkable updraft (the altitude of the 45-dBZ echo) and the presence of a substantial amount of supercooled water droplets and/or ice (the altitude of a strong reflectivity core above the zero-degree isotherm level).

Among the methods that combine radar measurements with other sources of meteorological data, the WAL method has the advantage of a relatively simple implementation. However, it should be noted that errors related to the height assigned to the measured reflectivities could have a negative influence on the performance of WAL algorithm. These errors result from radar beam size and from the limited number of elevation scans. Sampling errors can determine both an underestimation and an overestimation of the highest level at which a determined reflectivity value is observed. As an example, the presence, at long range, of large vertical reflectivity gradients may result in a relevant overestimation (Delobbe and Holleman, 2006).

In this work the freezing level has been derived from a linear interpolation of the radiosonde data acquired at Pratica di Mare station (41.67°N, 12.45°E), located at a distance of 150 km from the WR-10X site. In order to assess the representativeness of this station, a systematic comparison with the height of freezing level calculated from temperature data measured in Naples has been performed. From in situ measurements, the vertical temperature profile has been determined assuming a temperature decrease with height at the average lapse rate of 6.5°C per kilometer. Radiosoundings collected at Pratica di Mare proved to be very reliable in estimating the altitude of zero-degree isotherm level in the area of interest. Moreover, an estimate of the maximum error for linear interpolation of vertical temperature profiles measured by atmospheric soundings has been computed, in order to evaluate the possible impact of such error on WAL method performance. By using the classical mathematical formulation of error in linear interpolation (Davis, 1975), we computed the error bound associated to the linear interpolation of air-temperature data measured by radiosonde. Errors referring to the freezing point altitude range are discussed. In particular, we show results obtained for the interval (x_0, x_1), with x_0 and x_1 being respectively the altitudes where air-temperature is immediately above and below the freezing level. The frequency distribution of the error bound for the linear interpolation of air-temperature data in this interval is presented in Fig. 3.

The magnitude of error bound is generally lower than the total uncertainty in sounding (0.5°C) of radiosonde Vaisala RS92-SG temperature sensor used in Pratica di Mare station (Hurst et al., 2011). Therefore, the impact of error bound on the performance of WAL method can be considered negligible. However, the frequency distribution reveals rare cases in which the error in linear interpolation exceeds the value of 1.0°C. As worst scenario, we have considered the event in which the highest error bound (1.1°C) has been found. Assuming a temperature decrease with height at the average lapse rate of 6.5°C per kilometer, an error in air-temperature estimation of ± 1.1°C would result in an error of the altitude assigned to the freezing level of about ± 169 m. Thus, in the worst scenario the sensitivity of WAL algorithm to the error in linear interpolation of atmospheric sounding data can be considered negligible.

The present study aims to find not only the best threshold value for the height difference (i.e. a threshold that properly distinguishes between hail and severe rain), but also the reflectivity core where the WAL method exhibits the best

performances. In this respect, we applied WAL criterion computing Eq. (1) not only using H_{Z45}, but also as a difference between the maximum altitude attained by 35 and 40-dBZ reflectivity cores and H_{T0}.

.

2.2 Vertically-integrated liquid density method

The Vertically Integrated Liquid (VIL) was proposed as a proxy of storm cell severity by Greene and Clark (1972). The aim of the VIL product is to give an instantaneous estimate of the water content residing in an atmospheric layer. VIL converts reflectivity data (*Z*), which are the direct measurement of a weather radar, into equivalent liquid water content (*M*), through the semi-empirical relation between *M* (kg m^{-3}) and *Z* (mm^6 m^{-3}):

$$M = 3.44 \cdot 10^{-6}\, Z^{4/7} \tag{3}$$

Thereafter, the liquid water content is integrated vertically:

$$\mathrm{VIL} \equiv \int_0^{H_{top}} M \,\mathrm{dh} = 3.44 \cdot 10^{-6} \int_0^{\mathrm{H_{top}}} Z^{4/7} \,\mathrm{dh} \tag{4}$$

and has units of kilogram per square meter (kg m^{-2}). H_{top} is the maximum height of vertical layer, which depends on the distance from radar and elevation scan strategies.

When calculating VIL, several factors have to be taken into account. VIL values in storm located too close to the radar site are underestimate, because the radar is not able of scanning high enough to reach the upper portions of the thunderstorms (Brimelow et al., 2004). Problems are also encountered when making VIL measurements of storms occurring too far away from radar, because the relatively broad beamwidth of the radar could introduce uncertainties in the vertical resolution of the reflectivity data. Moreover, as highlighted in Delobbe and Holleman (2006), for highly tilted storms, the VIL product may be an unreliable indicator of the thunderstorm intensity. In this respect, a cell-based method that follows the cell vertically has been proposed in Stumpf et al. (2004). This approach could provide better assessment of VIL for tilted storms than the grid-based method (Brimelow el al., 2004). In the latter, before vertically integrating, the amount of liquid water from each elevation scan are mapped into a predetermined Cartesian grid.

To overcome some inherent problems with using VIL alone, Amburn and Wolf (1997) proposed the Vertically-Integrated Liquid Density (VIL-Density) radar product as hail indicator. VIL-Density can be obtained dividing the VIL by EchoTOP, which is the altitude (expressed in meters) of the highest bin measured by radar. The quotient is multiplied by 1000 in order to yield the results in (g m^{-3}):

$$\text{VIL-Density} = \frac{\text{VIL}}{\text{EchoTOP}}\ 1000 \quad (5)$$

VIL-Density can be useful for detect thunderstorms characterized by high reflectivities relative to their altitude; therefore, VIL-Density correlates well with storm cell containing hail cores. It is important to point out that VIL-Density only identify hail precipitation at high altitudes, since weather radar are not able to observe hail occurring on the ground. This problem may occur in cases of quite high freezing levels or if the hail encounters significant liquid water when falling.

3 Radar data and hail events

This section is aimed at describing the available X-band radar dataset and the methodologies used in the framework of quality control chain applied to WR-10X reflectivity measurements. In addition, the study area and the selected hail events are presented.

3.1 Radar data and quality control chain

WR-10X is a single-polarization radar manufactured by ELDES srl. In operative mode, WR-10X performs a volume scan with azimuth and range resolution of 3.0 degrees and 0.3 km, respectively, using a pulse repetition frequency of 800 Hz. WR-10X installation facility in Naples Castel Sant'Elmo is given in Fig. 4: a radome protects the parabolic type dish antenna, whose rotation rate is 20°/ second. The time for a full volume scan is about 3 minutes and the maximum available range is 72 km. The operational volume observation strategy, repeated every 10 minutes, includes 6 PPI sweeps, with antenna elevation angle ranging from 1 to 10 degrees.

Before any operational use, the raw radar reflectivity data have to be processed through a quality control chain. The latter is needed to mitigate some errors that affect the quality of radar measurements. Processing chain has been focused on some systematic errors that include biases and range-dependent effects, such as ground clutter residuals, backscatter from sea surface, beam blocking by surrounding topography and beam attenuation along the path (Capozzi et al., 2014).

In the WR-10X radar a statistical declutter filter is implemented, based on the different samples distribution between clutter echoes and meteorological echoes. This filtering procedure has been improved by means of a statistical filter, in order to eliminate the residual noise generated by ground clutter. The statistical filter is based on three main ingredients: entropy, texture and median filtering. The approach, used to suppress sea clutter noise, is based on vertical reflectivity profile analysis (Alberoni et al., 2001). Usually vertical reflectivity profiles are smooth and regular in rainy conditions, while in sea clutter condition a broken profile is often observed. A careful analysis of PPI at the lowest elevation angles showed the occurrence of sea clutter only at 1° (Capozzi et al., 2014): therefore, the analysis of vertical reflectivity profile involves the reflectivity measurements at 1° antenna elevation angle (Z_1) and 2° antenna elevation angle (Z_2). Sea clutter echoes are diagnosed when

the difference between Z_1 and Z_2 exceeds a determined threshold, assessed through the analysis of a great number of case studies. In order to minimize the effects of partial beam blockage caused by surrounding topography, we have applied the correction scheme proposed by Fulton et al. (1998). This scheme is applied to beams partially obstructed, i.e. only when the level of beam occultation lies between 10% and 60%, and consists of modifying the reflectivity factor measurements by adding 1 to 4 dBZ depending on the degree of occultation.

The two-way attenuation along the path, together with other sources of error, such as calibration errors, side lobe effects, shielding and range-dependent errors, can adversely affect the ability of weather radar to provide accurate measurements of vertical profile of reflectivity (Delobbe and Holleman, 2006). This issue has a significant relevance at X-band (e.g. Delrieu et al. 1999a, b) and it is strongly dependent on rain rate (Marzano et al., 2003). Nowadays, the most efficient approach to estimate the attenuation of the returning radar echoes is based on the differential phase shift between the vertical and horizontal orthogonal phases (e.g. Smyth and Illingworth, 1998), i.e. on a method that takes advantage of dual-polarization weather radar features. The weather radar tested in this work, being a single-polarization system, cannot exploit polarimetric capabilities. In the framework of the quality control chain applied to correct WR-10X reflectivity measurements, the beam attenuation along the path has been mitigated through a classical iterative procedure that involves the estimation of two-way path integrated attenuation (PIA) along the entire beam path. This iterative algorithm has been tested for strong and moderate rainfall events, in which attenuation problem can be of particular relevance (Capozzi et al., 2014). The PIA iterative method proved to be reliable in attenuation correction within a range (i.e. distance from the radar site) less than 50 km; occasional failures of this methodology have been observed in the case of particular meteorological scenarios, characterized by moderate and persistent rainfall in the range closest to the radar site. In the specific context of our study the influence of path attenuation on radar-based hail detection techniques performance may be considered relatively low because the radar-based hail detection products, developed in this work, have been tested at urban scales of the order of few tens of kilometers. The occurrence of path attenuation along specific radial directions may be considered relatively rare at short ranges (Marzano et al., 2012) and, therefore, not affecting the performance of X-band radars, at least in a statistical sense. In addition, in order to minimize the effects of attenuation, we have focused the selection of thunderstorm events on situations where no other convective cells are present along the radial directions between the radar site and the convective cell of interest.

In order to implement the WAL method, ΔH has been determined using the maximum height of 45-dBZ reflectivity core, according to Eq. (1). From corrected radar volumes, the latter has been computed for each azimuth and range as the altitude of the highest radar beam where a reflectivity at least equal to 45-dBZ is measured. In the same manner, ΔH has been computed also for the 35 and 40-dBZ reflectivity cores. In order to implement the VIL-Density method, corrected reflectivity data Z have been converted into liquid water content (M) according to Eq. (3). In the next step, liquid water content has been integrated over each vertical column, using Eq. (4), to find the VIL product. Finally, VIL-Density has been calculated through Eq. (5), using VIL values and EchoTOP heights. For each radar training dataset, the radar polar volumes have been resampled onto a uniform Cartesian grid with 1-km horizontal resolution and 0.5-km vertical resolution before the integration for VIL calculation.

3.2 Study area and hail events

The area covered by radar measurements includes the western sector of Campania Region, as highlighted by Fig. 5. In this area, thunderstorm events occur all year round; in the warm season (May to October), convection is mainly triggered by the interaction between small-scale mechanism and synoptic-scale flow, while in cold season (November to April) it is associated with the passage of a cold front or with a cold occlusion. The analyzed region is bounded on the north by Matese mountains and on the east by Campania Apennine, which have height values of more than 2000 and 1500 m, respectively. These two orographic features constitute an important factor in the mesoscale meteorology of the region, enhancing convection systems development, especially in summer season. Sea-air interactions also play a crucial role in storm activity: in the early part of fall season, when sea surface temperatures reach the maximum value (≅ 26°C), coastal areas are sometimes affected by heavy thunderstorms, that are able to produce considerable rainfall accumulation (> 100 mm) in a relatively short time. During warm season, convection can be even triggered by the low-level convergence between diurnal sea-breeze and synoptic-scale flow, when an unstable environment is present. This mechanism usually occurs in the inland sectors (at a distance of about 20-30 km from the coast) and, in combination with orographic forcing, can cause the development of hail producing thunderstorms.

The database used in this work includes 53 thunderstorms that occurred in the study area from April 2012 through June 2015. Other events have been discarded since thunderstorms were not well detected by the radar scans; this is due to beam blocking at lower elevations, especially along volcano Vesuvio direction (i.e. in the southeastern sectors of the area of interest). On the other hand, for thunderstorms that took place within the cone of silence (that is, near to the radar site), WR-10X is not able to scan the upper part of the thunderstorm, thus WAL and VIL-Density methods cannot be applied effectively.

Hail was produced by 34 thunderstorms, while the remaining 19 produced heavy rain mixed with few hailstones or without hail at all. Days with thunderstorm and hail occurrence in the examined period have been identified by means three Synop stations, belonging to the network of "Meteorological Service of Military Italian Aeronautics", whose data are available on an hourly basis. Because of the restricted spatial extension of the majority of hail events, the Synop observers reported only a small sample of the total number of events. Therefore, in order to complete the ground truth data, reports of hail events provided by volunteers and local papers have been taken into account. However, some locations and times listed on volunteers' reports may not be accurate and some spotters may not have given their exact latitude and longitude. Moreover, some hail events may have occurred in places were spotters were not available. The location of the 34 hail reports is presented in Fig. 6: in order to highlight the verification data type (volunteers report, Synop observation and local newspapers), different markers have been used. The Synop observations (five in all) have been all provided by Naples / Capodichino station (40.8848°N, 14.2917°E).

To reduce spatial mismatching effects, the comparison between the outputs of two algorithms and in situ hail reports has been performed selecting radar pixels falling within 15-km distance from hail report location. Among these pixels, the one

with highest ΔH value in Eq. (1) and the one with highest VIL-Density in Eq. (5) have been considered. In order to reduce also temporal mismatching effects, at both ends of the time window observation a tolerance of 10 minutes has been applied.

Table 1 and Table 2 show the distribution of the number of thunderstorm events, with and without hail, for given ranges of ΔH and VLD, respectively. As expected, the number of events without hail decreases as ΔH and VLD values increase. For ΔH values greater of 1.0 km, almost all producing-hail thunderstorms have been recorded, while for ΔH less than 1.0 km most of thunderstorm events observed did not cause hail. For VLD values greater of 3.5 g m^{-3}, only producing-hail thunderstorms have been observed, while for VLD less than 2.5 g m^{-3} most of thunderstorm events recorded did not cause hail.

Seasonal analysis results (Table 3) highlight some of the thunderstorm features above described. Hot season (May to October) events, developing in a moist and warm environment, are characterized by greater VIL, VLD and ΔH median values than those found for cold season (November to April). Consequently, warm season thunderstorm events, having a deeper vertical extension, are more prone to produce dangerous hailstones. However, hail formation processes are strongly related not only with cloud height and updrafts magnitude, but also with the cloud depth below the freezing level (Pappas, 1962). In this respect, the lower freezing level found for winter cases can enhance the production of hail stones, although smaller and less dangerous than those of warm season events, because a greater depth of the thunderstorm could have sub-freezing temperatures.

4 Methodology and results

This section is devoted to the brief description of the verification methodology, the set up of the proposed X-band technique for estimating the probability of hail and, as an example, the application of the latter to a recent hail event.

4.1 Verification scores

The comparison of the outcomes of the two selected methodologies and ground-truth hail reports was primarily concerned with finding a warning threshold that would correctly identify the hail cases with a minimum of false alarms. Thunderstorms events have been classified using a 2-by-2 contingency table (Table 4). The meaning of symbolisms adopted in Table 4 is explained below:

- **H (hit)** is an integer that represents the number of times that a hail event is detected by a radar-based method and is observed by ground truth reports;
- **F (false alarm)** is an integer that represents the number of times that a hail event is detected by a radar-based method and is not observed by ground truth reports;

- **M (miss)** is an integer that represents the number of times that a hail event is not detected by a radar-based method and is observed by ground truth reports;
- **N (corrected negative)** is an integer that represents the number of times that a hail event is not detected by a radar-based method and is not observed by ground truth reports.

It is assumed that a hail event is detected by a radar-based method, e.g. the WAL technique, when ΔH is above a certain threshold. In this work, in order to find the optimal warning thresholds for hail warning in Naples urban area, the contingency table has been computed for several values of ΔH, ranging from 0.2 and 3.0 km, and for several VLD values, ranging from 1.4 to 5.4 g m^{-3}.

By adopting the outcomes of the 2-by-2 contingency table, the following statistical scores have been computed:

$$\text{Probability of Detection (POD)} = \frac{H}{H+M} \quad (6)$$

$$\text{False Alarm Ratio (FAR)} = \frac{F}{H+F} \quad (7)$$

$$\text{Critical Success Index (CSI)} = \frac{H}{H+M+F} \quad (8)$$

$$\text{Probability Of Hail (POH)} \equiv \frac{H}{H+F} = 1\text{-FAR} \quad (9)$$

The main features of those scores are presented in Table 5. The CSI summarizes the verification result in a single number and has been used to determine a good forecast decision threshold.

4.2 Statistical analysis and probability-of-hail index

Figure 7 shows, for the two selected methods, the behavior of the scoring indexes values (POD, FAR, CSI and POH) depending on their warning thresholds. For the WAL method, the results obtained using 35-dBZ (WAL 35-dBZ), 40-dBZ (WAL 40-dBZ) and 45-dBZ (WAL 45-dBZ) reflectivity cores to compute ΔH are presented. The behavior of scoring parameters are quite similar for the two algorithms. The results highlighted a lowering of both POD and FAR with increase of thresholds and that CSI reaches the maximum value at a determined threshold. However, for WAL 35 and 45-dBZ a slight increase in FAR score has been observed for threshold values greater than 1.5 km. The highest CSI value (0.82) was obtained for the WAL 40-dBZ method. Using this reflectivity core, the CSI maximizes for ΔH = 1.0 km, which corresponds to a POD of 0.91 and to a

FAR of 0.11. This ΔH threshold correctly detects as hail producing the 91% (31 of 34) of the thunderstorm events occurred in the examined period and falsely identifies as hail producing the 21% (4 of 19) of the thunderstorms without hail. For the WAL 45-dBZ method, CSI score maximizes for a height difference threshold (0.6 km) slightly lower than that carried out for the other two WAL criteria.

As concerning the VIL-Density method, the highest CSI (0.76) has been observed using a warning threshold of 2.4 g m^{-3}. This VLD threshold appears to be reasonable, identifying all of the hail producing thunderstorms. However, the FAR score carried out for this method (0.24) is higher than that found for the WAL 40-dBZ algorithm. The optimal VLD threshold for hail occurrence found in this study is much lower than those discovered in the previous studies (e.g. Amburn and Wolf, 1997; Rose and Troutman, 1997; Roeseler and Wood, 2001; Lahiff, 2005). The results obtained from these studies show that VLD threshold values which correctly identify the hail-producing storms are within a range between 3.1 and 3.7 g m^{-3}. However, the threshold values for a specific area can be affected by issues such as topography, height of the radar above sea level and the local climatic context. Therefore, the present work confirms that, in order to make an optimal use of VIL-Density, it is important to perform a local study aiming to find the best thresholds value for a determined area (Lahiff, 2005).

In order to determine a POH index, that can be easily used into an operative framework to assess the hail warning in Naples urban area, we have modeled the relationship between POH score and the radar products ($\Delta H = H_{Z40} - H_{T0}$ for WAL method and VLD for VIL-Density technique) by using a third-order polynomial fit. We set up the polynomial model using POH score as dependent variable and the radar product (ΔH or VLD) as independent variable:

$$POH_{WAL} = p_1 (\Delta H)^3 + p_2 (\Delta H)^2 + p_3 (\Delta H) + p_4 \quad (10)$$

$$POH_{VLD} = c_1 (VLD)^3 + c_2 (VLD)^2 + c_3 (VLD) + c_4 \quad (11)$$

The best fit between ΔH thresholds and POH score is obtained when $p_1 = 0.1181$, $p_2 = -0.5291$, $p_3 = 0.7821$ and $p_4 = 0.4975$ (Fig. 8a). For VIL-Density method, the best fit is achieved when $c_1 = 0.009344$, $c_2 = -0.1106$, $c_3 = 0.5057$, $c_4 = 0.05351$ (Fig. 8b). Using the warning thresholds identified through the statistical analysis (ΔH = 1.0 km and VLD = 2.4 g m^{-3}), the two optimal values for hail warning in Naples urban area have been determined, $POH_{WAL} = 0.87$ and $POH_{VLD} = 0.76$. Therefore, for an operative use, for WAL method, when POH_{WAL} is greater than 0.87 (87% in percentage), a hail event is occurring. In the same manner, for VIL-Density method, when POH_{VLD} is above 0.76 (76%), hail precipitation is occurring.

4.3 Application to case study on 21 July 2014

A severe hailstorm occurred on 21 July 2014 in the Sorrentine Peninsula, a region that separates the Gulf of Naples to the north from the Gulf of Salerno to the south. The synoptic situation, very unusual for the summer season, was characterized by a low-pressure system over the northern Italy, affecting the Central Mediterranean basins (Fig. 9, left panel). This low determined a

cold air advection over the northern and central sectors of Italian peninsula and a warm and moist meridional flow over southern Tyrrhenian sea. Therefore, the study area was located along the boundary of the two adjacent air masses. This thermal boundary was associated with a low-level wind convergence line, with a jet-stream in the upper levels and was characterized by a strong advection of moisture. Those factors promoted a strong convective forcing, as is often observed for Mediterranean heavy precipitating events (Lebeaupin et al., 2006). Moreover, as usual in summer season, sea surface temperature was high (24°C) in the area of interest and favored evaporation, which supplied moisture to the low-levels as well as increasing the convective instability. According to Pratica di Mare radio-sounding data collected at 12:00 UTC, the isotherm of zero degree was roughly 3500 m a.s.l. in the area of interest.

Images from satellite and WR-10X weather radar give useful information about the initiation and the evolution of the hailstorm. The latter developed in the early afternoon (at 14:30 UTC) offshore of Naples Gulf, along the thermal boundary above described. According to Meteosat Second Generation visible (0.6 μm) image (Fig. 9, right panel), a V-shaped structure of the thunderstorm can be assumed at 15:30 UTC. The latter indicates the presence of a strong updraft, which was blocking the horizontal south-western flow: as the wind was forced around the updraft, it created a V-shaped structure, whose horizontal extension was around 120 km. Figure 10 displays a sequence of WR-10X images (showing Vertically Maximum Intensity, i.e. the maximum reflectivity value on the vertical of every point) that allows to obtain a time history of hailstorm displacement. The thunderstorm cell showed its first clear signature on radar images at 14:35 UTC. In next 90 minutes, the cell rapidly moved from southwest to northeast, affecting the Gulf of Salerno and the southern sector of Naples Gulf. The convective system reached its peak intensity between 15:25 and 15:45 UTC, causing heavy rainfall and hail in Sorrento and Vico Equense cities. Within the area most affected by the hailstorm, there was one automatic rain-gauge, located in Sorrento city (40.62997 N, 14.38238 E). This rain-gauge recorded a total accumulation of 29.2 mm in one hour (from 15:00 to 16:00 UTC). The passage of the thunderstorm core produced an amount of 16.8 mm in a ten-minutes period (15:40-15:50 UTC), with rain rates up to 33 mm/10 min. According to local newspaper (Il Mattino, July 21, 2014), hail precipitation lasted about 15 minutes, causing tangible damages to transport activities and crops. The hailstones had a diameter of up to 3-4 cm (Fig. 11), but no significant accumulation on the ground was observed.

When the hailstorm core passed over Sorrento city, it was characterized by ΔH (= $H_{Z40} - H_{T0}$) values up to 1.5 km (Fig. 12a). Those values suggest that convective cell had a great vertical extension, that was favorable to the hail stones growth. In this respect, the presence of 40-dBZ echoes well above the zero degree level is a clear signature of a strong, wide and persistent updraft in the hail stones growth layer (-10°C to -30°C). In addition, VLD values up to 3.5 g m^{-3} (Fig. 12c) also indicate the presence of a deep and intense hail core. Using Eq. (10) and Eq. (11), POH products for WAL 40-dBZ (Fig. 12b) and VIL-Density (Fig. 12d) methods have been generated, respectively. POH index, expressed as percentage, ranges from 0% (no chance of hail) to 100% (certainty of hail). According to on-ground reports and observations, in the area of Sorrento a very high probability of hail (≅ 88% for WAL 40-dBZ and ≅ 80% for VIL-Density) has been detected above the thresholds found in the previous paragraph. Therefore, in this case both POH indexes proved to be reliable in hail core identification.

5 Conclusions

The main aim of this study is to develop a hail detection algorithm, based on the measurements of a single-polarization X-band weather radar, in order to provide a real-time hail warning in Naples metropolitan area. The dataset, used in this work, includes 53 thunderstorm events, occurred in the study area between April 2012 and June 2015. The information about hail phenomena at ground level have been collected using the observations provided by three Synop stations, the volunteer's reports and the newspapers. Due to the small spatial and temporal extent of most hail events, the latter two sources of information proved to be very useful to generate a sufficiently large dataset of on-ground hail observations. Among various methods proposed in literature, the Waldvogel algorithm and the Vertically-Integrated Liquid Density method have been selected to identify hail from reflectivity data measured by X-band weather radar operating in Naples urban area. The first one relies on the difference (ΔH) between the maximum altitude attained by the 45-dBZ echo and the height of zero-degree isotherm. The capabilities of this method have been evaluated computing ΔH not only for the 45-dBZ reflectivity core, but also for the 35-dBZ and 40-dBZ cores. The output (VLD) of the second method is derived exclusively from radar scans and is obtained dividing the VIL, that is an estimate of the water content residing in an atmospheric layer, by the EchoTOP, the altitude of the highest bin measured by radar. The outcomes of the two radar-based hail detection criteria have been compared with ground truth observations, using a statistical scores technique based on a 2x2 contingency table. The verification analysis allowed obtaining ΔH and VLD thresholds that would reliably detect hail events with a minimum of false alarms and misses. For the Waldvogel method, the best results have been obtained for 40-dBZ reflectivity core: using this reflectivity value, the Critical Success Index (CSI), that summarizes the verification results in a single number, maximizes for ΔH = 1.0 km. For Vertically-Integrated Liquid Density method, the highest value for CSI was reached for VLD = 2.4 g m^{-3}. These thresholds have proven to be reliable in identifying the hail producing thunderstorms, detecting the 91% and 100% of the thunderstorms with hail occurred in examined period, respectively. However, from operational perspective, the FAR score found for Vertically-Integrated Liquid Density method (24%) looks quite high and should be improved.

The relationship between the Probability of Hail (POH) and the output of the two hail detection criteria has been derived through a heuristic approach, using a third-order polynomial fitted curve. This relationship can be used in operational mode to convert ΔH and VLD values into a POH index, varying between 0 and 100%. An example of POH indexes performance has been shown for a hail event occurred on 21 July 2014 in the Sorrento Peninsula. In this case, both hail detection methodologies have proven to be reliable in hail core identification.

The results obtained from this study are very encouraging and can bring benefits for risk management associated to hail events. Future work shall be devoted to reduce the FAR score found for Vertically-Integrated Liquid Density; in this respect, more intercomparisons between radar and ground truth observations will be carried out to cover a larger number of events. Moreover for future analysis, in order to improve the hail detection products performance close to the radar site, the operational volume observation strategy will include more PPI sweeps at higher elevations angles.

Data availability

The WR-10X radar data used in this work can be accessed through the website of "Campania Center for Marine and Atmospheric Monitoring and Modelling" of the University of Naples "Parthenope" (meteo.uniparthenope.it).

Radiosonde data collected in Pratica di Mare (16245 LIRE) are provided by the Department of Atmospheric Science, University of Wyoming (weather.uwyo.edu/upperair/sounding.html).

The Synop reports used to identify thunderstorm and hail occurrence in the study area can be accessed through the following website: www.ogimet.com/synops.phtml.en.

Acknowledgments

The authors thank the "Soprintendenza Speciale per il Patrimonio Storico Artistico ed Etnoantropologico e per il Polo Museale della città di Napoli" for hosting the weather radar at Castel Sant'Elmo. ELDES srl (Florence, Italy) personnel is acknowledged for technical support. The authors are very grateful also to Campania Region Department of Civil Protection (DPC), Naples, Italy, for having kindly granted the access to rainfall data acquired by their monitoring rain-gauge network.

References

Alberoni, P. P., Andersson, T., Mezzasalma, P., Michelson, D. B., and Nanni, S.: Use of the vertical Reflectivity profile for Identification of Anomalous propagation, Meteorol. Appl., Vol. 8 (3), pp. 257 – 266, 2001.

Amburn, S.A. and Wolf, P.L.: VIL Density as a hail indicator, Wea. Forecasting, Vol. 12, pp. 473-478, 1997.

Anagnostou, E.N., Anagnostou, M.N., Krajewski, W., Kruger, A., and Miriovsky, B.: High-resolution rainfall estimation from X-band polarimetric radar measurements. J. Hydrometeor., vol. 5, pp. 110–128, 2004.

Auer, A.H.: Hail recognition through the combined use of radar reflectivity and cloud-top temperatures, Mon. Wea. Rev., Vol. 122, pp. 2218-2221, 1994.

Aydin, K., Seliga, T.A., and Balaji, V.: Remote sensing of hail with a dual linear polarization radar, J. Appl. Meteor., Vol. 25, pp. 1475-1484, 1986.

Brimelow, J.C., Reuter, G.W., Bellon, A., and Hudak, D.: A radar-based methodology for preparing a severe thunderstorm climatology in central Alberta, Atmosphere-Ocean, Vol. 42:1, pp. 13-22, 2004.

Capozzi, V., Picciotti, E., Budillon, G., and Marzano, F.S.: X-band weather radar monitoring of precipitation fields in Naples urban areas: data quality, comparison and analysis, The Eighth European Conference On Radar in Meteorology and Hydrology, 2014.

Capozzi, V., Mazzarella, V., Moccia, M., Picciotti E., Budillon, G., and Marzano, F.S.: Hail detection in Naples urban area using single-polarization X-band weather radar: Preliminary results. In: Metrology for Aerospace (MetroAeroSpace), 2015 IEEE Xplore Digital Library, pp. 289-294, 2015.

Davis, P.J.: Interpolation and approximation, Dover, reprint, pp. 108-126, 1975.

Delobbe, L., Dehenauw, D., Hamid, K., and Heméghaire, G.: Hail detection using radar observations: case studies in the summer 2002, Royal Meteorological Institute of Belgium, 2003.

Delobbe, L. and Holleman, L.: Uncertainties in radar echo top heights used for hail detection, Meteorol. Appl., Vol. 13, pp. 361-374, 2006.

Delrieu, G., Hucke, L., and Creutin, J.D.: Attenuation in Rain for X- and C-Band Weather Radar Systems: Sensitivity with respect to the Drop Size Distribution, Journal of Applied Meteorology, Vol. 38, pp. 57-68, 1999a.

Delrieu, G., Serrar, S., Guardo, E., and Creutin, J.D.: Rain Measurement in Hilly Terrain with X-Band Weather Radar Systems: Accuracy of Path-Integrated Attenuation Estimates Derived from Mountain Returns, J. Atmos. Oceanic Technol., Vol. 16 pp. 405–416, 1999b.

Fulton, R.A., Breidenbach, J.P., Seo, D., Miller, D., and O'Bannon, T.: The WSR- 88D Rainfall Algorithm, Wea. Forecasting, Vol. 13, pp. 377-395, 1998.

Geotis, S.G.: Some radar measurements of hailstorms, F. Appl. Meteorol., Vol. 2, pp. 270-275, 1963.

Greene, D.R. and Clark, R.A.: Vertically integrated liquid water – a new analysis tool, Mon. Wea. Rev., Vol. 100, pp. 548-552, 1972.

Holleman, I.: Hail detection using single-polaritazion radar, Scientific Report, KNMI WR-2001-01, 2001.

Hurst, D. F., Hall, E. G., Jordan, A. F., Miloshevich, L. M., Whiteman, D. N., Leblanc, T., Walsh, D., Vömel, H., and Oltmans, S. J.: Comparisons of temperature, pressure and humidity measurements by balloon-borne radiosondes and frost point hygrometers during MOHAVE-2009, Atmos. Meas. Tech., 4, 2777-2793, doi:10.5194/amt-4-2777-2011, 2011.

Il Mattino: Grandinata record a Sorrento, i chicchi enormi danneggiano i campi, retrieved from http://www.ilmattino.it/napoli/cronaca/grandinata_sorrento_foto_video-508584.html, July 21, 2014.

Kunkel, K.E., Karl, T.R., Brooks, H., Kossin, J., Lawrimore, J.H., Arndt, H., Bosart, L., Changnon, D., Cutter, S.L., Doesken, N., Emanuel, K., Groisman, P.Y., Katz, R.W., Knutson, T., O'Brien, J., Paciorek, C.J., Peterson, T.C., Redmond, K.,

Robinson, D., Trapp, J., Vose, R., Weaver, S., Wehner, M., Wolter, K., and Wuebbles, D.: Monitoring and Understanding Trends in Extreme Storms: State of Knowledge. Bull. Amer. Meteor. Soc., 94, 499–514, 2013.

Lahiff, C.N.: Vertically Integrated Liquid Density and its associated hail size range across the Burlington, Vermont County warning area, Eastern Region Technical Attachment, No. 05-01, 2005.

Lebeaupin, C., Ducrocq, V., and Giordani, H.: Sensitivity of torrential rain events to the sea surface temperature based on high-resolution numerical forecasts, J. Geophys. Res. 111 (D12), 1211, 2006.

Mallafre, M.C., Ribas, T.R., LlsatBotuja, M.C., and Sanchez, J.L.: Improving hail identification in the Ebro Valley region using radar observations: probability equations and warning thresholds, Atmo. Res., Vol. 93, pp. 474-482, 2009.

Marzano, F.S., Roberti, L., Di Michele, S., Tassa, A., and Mugnai, A.: Modeling of apparent radar reflectivity due to convective clouds at attenuating wavelengths. Radio Sci., Vol. 38, pp. 1002, 2003.

Marzano F.S., Scaranari, D., and Vulpiani, G.: Supervised fuzzy-logic classification of hydrometeors using C-band dual-polarized radars. IEEE Trans. Geosci. Rem. Sensing, ISSN: 0196-2892, n. 45, pp. 3784-3799, 2007.

Marzano, F.S., Botta G., and Montopoli M.: Iterative Bayesian Retrieval of Hydrometeor Content from X-band Polarimetric Weather Radar. IEEE Trans. Geosci. Rem. Sensing, Vol. 48, pp. 3059-3074, 2010.

Marzano, F.S., Budillon, G., Picciotti, E., Montopoli, M., Zinzi, A., and Buonocore, B.: X-band weather radar monitoring real-time products in Rome and Naples urban areas. Tyrrhenian Workshop 2012 on Advances in Radar and Remote Sensing, 2012.

Matrosov, S.Y., Kingsmill, D.E., Martner, B.E., and Ralph, F.M.: The utility of X-band polarimetric radar for quantitative estimates of rainfall parameters. J. Hydrometeorol., Vol. 6, pp. 248–262, 2005.

Montopoli M., Picciotti, E., Telleschi, A., and Marzano, F.S.: X-band weather radar monitoring of precipitation fields at urban scale: spatial calibration and accuracy evaluation. Proc. of the 6th European Conference on Radar in Meteorology and Hydrology (ERAD), Sibiu (Romania), 2010.

Pappas, J.J.: A Simple Yes-No Hail Forecasting Technique, Journal of Applied Meteorology, Vol. 1, pp. 353-354, 1962.

Roeseler, C. A. and Wood, L.: VIL Density and Associated Hail Size along the Northwest Gulf Coast, NWS Southern Region Local Research Project: Houston, TX and Lake Charles, LA, 2001.

Rose, M.A. and Troutman, T.W.: An Examination of VIL and Echo Top Associated with Large Hail in Middle Tennesse, NWS Southern Region Technical Attachment No. - 12 - 97-15. Nashville, TN, 1997.

Skripniková, K. and Řezáčová, K.: Radar-based hail detection, Atmospheric Research, Vol. 144, pp. 175-185, 2014.

Smyth, T.J. and Illingworth, A.J.: Correction for attenuation of radar reflectivity using polarization data, Quarterly journal of the Royal Meteorological Society, Vol. 124, Issue 551, pp. 2393–2415, Oct. 1998 Part A.

Straka, J.M., Zrnic, D.S., and Ryzhkov, A.V.: Bulk hydrometeor classification and quantification using polarimetric radar data. Synthesis of relations, J. Appl. Meteor., Vol. 39, No. 8, pp. 1341-1372, Aug. 2000.

Stumpf, G.J., Smith, T.M., and Hocker, J.: New hail diagnostic parameters derived by integrating multiple radars and multiple sensors, Preprints 22nd Conf. on Severe Local Storm, Hyannis, MA., Amer. Meteor. Soc., P7.8, 2004.

Tilford, K.A., Fox, N.I., and Collier, C.G.: Application of weather radar data for urban hydrology, Meteorological Applications, Vol. 9, Issue 1, pp. 95-104, 2002.

Van de Beek, C. Z., Leijnse, H., Stricker, J. N. M., Uijlenhoet, R., and Russchenberg, H. W. J.: Performance of high-resolution X-band radar for rainfall measurement in The Netherlands. Hydrol. Earth Syst. Sci., Vol. 14, pp. 205-221, 2010.

Waldvogel, A., Federer, B., and Grimm, P.: Criteria for the detection of hail cells, J. Appl. Meteor., Vol. 18, pp. 1521 1525, 1979.

Witt, A., Eilts, M.D., Stumpf, G.J., Johnson, J.T., Mitchell, E.D., and Thomas, K.W.: An enchanced hail detection algorithm for the WSR-88D, Wea. and Forecasting, Vol. 13, pp. 286-303, 1998.

Table 1. Number of thunderstorms with and without hail for given ranges of ΔH. The results obtained computing ΔH with the three different reflectivity cores used in this study (35, 40 and 45-dBZ) are presented.

Events occurred in 2012-2015 period	Range in ΔH (km)														
	<= 0.5			0.6 – 1.0			1.1– 1.5			1.6 – 2.0			>= 2		
	35 dBZ	40 dBZ	45 dBZ	35 dBZ	40 dBZ	45 dBZ	35 dBZ	40 dBZ	45 dBZ	35 dBZ	40 dBZ	45 dBZ	35 dBZ	40 dBZ	45 dBZ
Number of events with hail	3	3	1	2	1	7	6	9	9	6	7	6	17	14	8
Number of events without hail	7	11	7	4	4	4	1	1	1	1	0	1	4	2	2

Table 2. Number of thunderstorms with and without hail for given ranges of VLD.

Events occurred in 2012-2015 period	Range in VLD (g m^{-3})				
	< 2.5	2.5 – 3.5	3.6 – 4.0	4.1 – 4.5	> 4.5
Number of events with hail	3	13	10	2	6
Number of events without hail	7	11	1	0	0

Table 3. Median value of some products generated by the two radar-based hail detection algorithms for warm season events (May to October) and for cold season events (November to April).

Events occurred in 2012-2015 period	VIL ($kg\ m^{-2}$)	VLD ($g\ m^{-3}$)	H_{T0} (m)	H_{Z35}-H_{T0} (m)	H_{Z40}-H_{T0} (m)	H_{Z45}-H_{T0} (m)
Warm season events (May to October)	8.3	3.5	3400	2850	2250	1850
Cold season events (November to April)	4.6	3.0	1800	1300	1250	1000

Table 4. 2-by-2 contingency table used in the comparison between the outcomes of the two different radar-based hail detection methods and the ground truth verification data.

		Has the hail event been detected by radar?		
		YES	NO	
Has the hail event been observed on the ground?	YES	H (Hits)	M (Misses)	Total number of events observed on ground H+M
	NO	F (False Alarms)	N (Corrected Negatives)	Total number of events not observed on ground F+N
		Total number of hail events detected by radar H+F	Total number of hail events not detected by radar M+N	Total number of events H+F+M+N

Table 5. Main peculiarities of the statistical scores determined from the outcomes of the 2-by-2 contingency table, the Probability of Detection (POD), the False Alarm Ratio (FAR), the Critical Success Index (CSI) and the Probability of Hail (POH).

Score	Range of values	Features	Example
POD	from 0 to 1	It is sensitive to hits (H) and does not consider false alarms (F). It represents the fraction of hail events correctly detected by radar (H) with respect to the total number of hail events observed on ground (H+M).	POD = 0.7 means that the 70% of the hail events observed on ground has been correctly detected by radar.
FAR	from 0 to 1	It is sensitive to false alarms (F). It represents the fraction of hail events detected by radar but not observed by ground truth reports.	FAR = 0.25 means that the 25% of the hail events detected by radar has not been observed on ground
CSI	from 0 to 1	It is sensitive to both F and M. It represents the fraction of hail events observed on ground and/or detected by radar that have been correctly detected by radar.	CSI = 0.6 means that the 60% of the hail events observed on ground and/or detected by radar has been correctly detected by radar
POH	from 0 to 1	It is sensitive to both H and F. It represents the fraction of hail events correctly detected by radar with respect to the total number of hail events detected by radar (H+F).	POH = 0.5 means that the 50% of hail events detected by radar has been observed on ground.

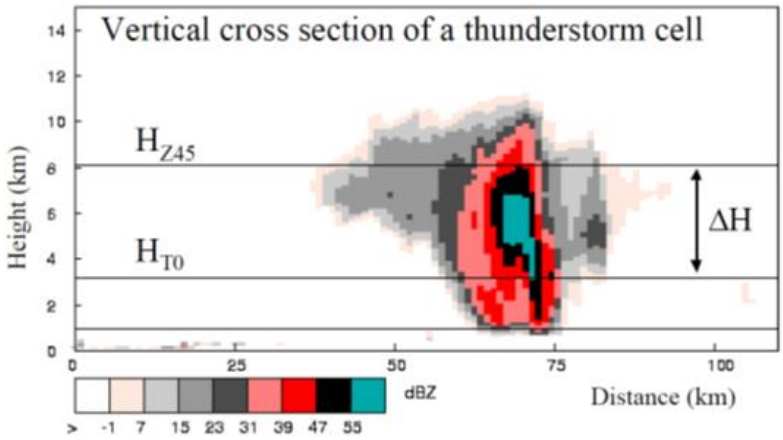

Fig. 1. Criterion of hail detection proposed in Waldvogel et al. (1979). The latter is based on the difference (ΔH) between a radar height signature for strong updraft and large amounts of hydrometeors (H_{Z45}) and the freezing level (H_{T0}).

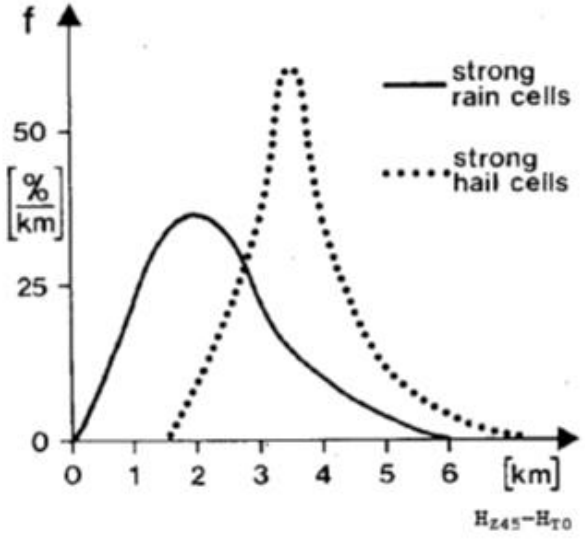

Fig. 2. Normalized frequency distributions of the parameter (H_{Z45}-H_{T0}) for strong rain cells and strong hail cells.

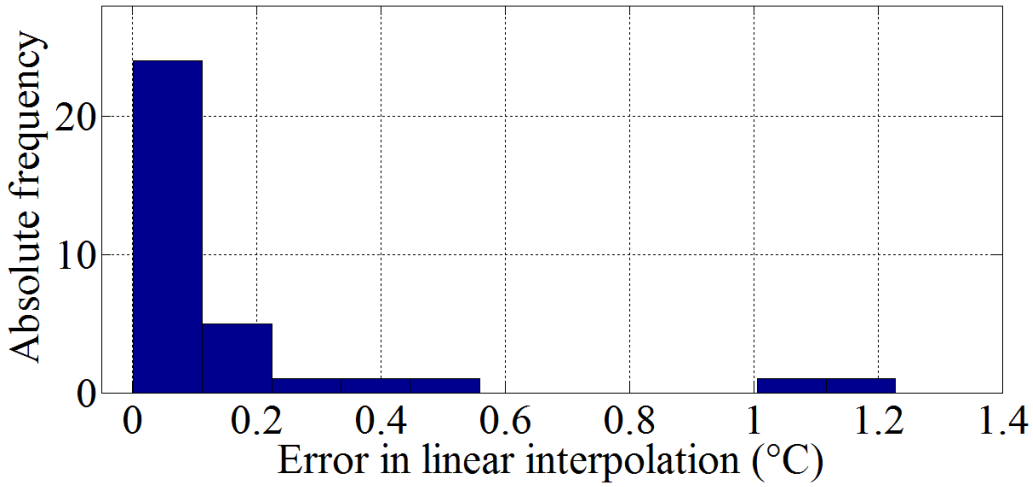

Fig. 3. Frequency distribution of error bound for linear interpolation of temperature data measured by atmospheric soundings in the altitudes interval (x_0, x_1) where the freezing level is located. x_0 and x_1 are respectively the altitudes where air-temperature is immediately above and below the freezing level.

Fig. 4. WR-10X installation at Naples Castel Sant'Elmo site.

Fig. 5. Map of study region including radar location (filled-in red circle). Circular line at 72 km from Naples Castel Sant'Elmo indicates the limit of the area covered by radar.

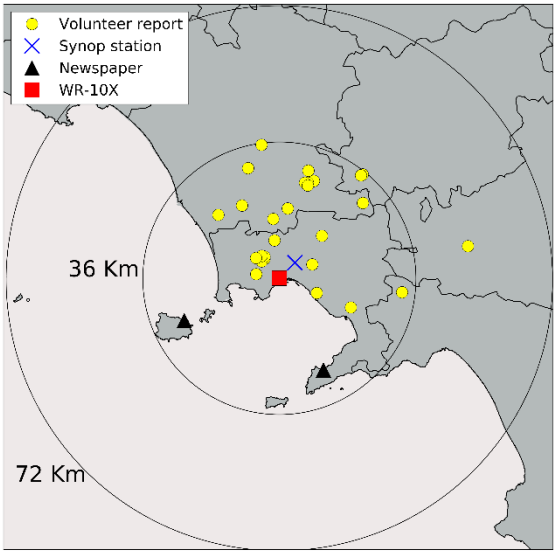

Fig. 6. Location of ground hail events occurred in the study area in the period April 2012-June 2015. The hail reports provided by volunteers are marked as filled-in yellow circle, those provided by Synop observations as blue cross and the reports from local newspaper as filled-in black triangle. The Synop observations (five in all) have been all provided by Napoli / Capodichino station (40.8848°N, 14°2917°E). WR-10X location is highlighted as filled-in red square.

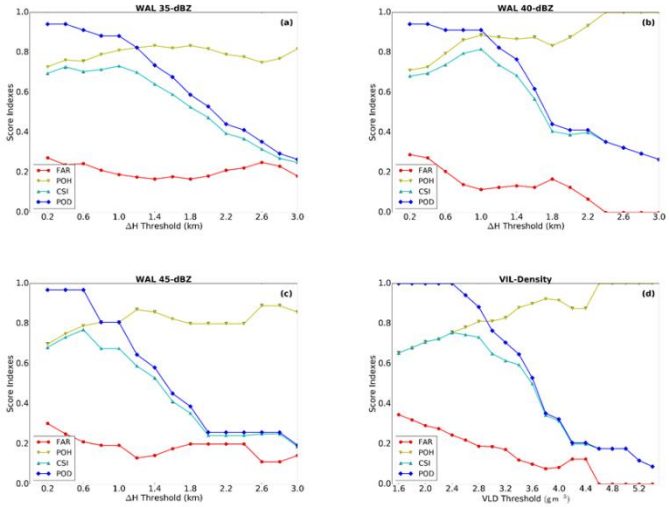

Fig. 7. The scoring parameters (FAR, POH, CSI and POD) for the two hail detection methods as a function of the warning threshold. In (a), (b) and (c), the results obtained for the WAL method using the three reflectivity cores (35, 40 and 45 dBZ) tested in this study to compute ΔH are presented. In (d) the results obtained for VIL-Density criterion are shown. The scoring parameters are deduced from the comparison of the two methods with ground-truth verification data.

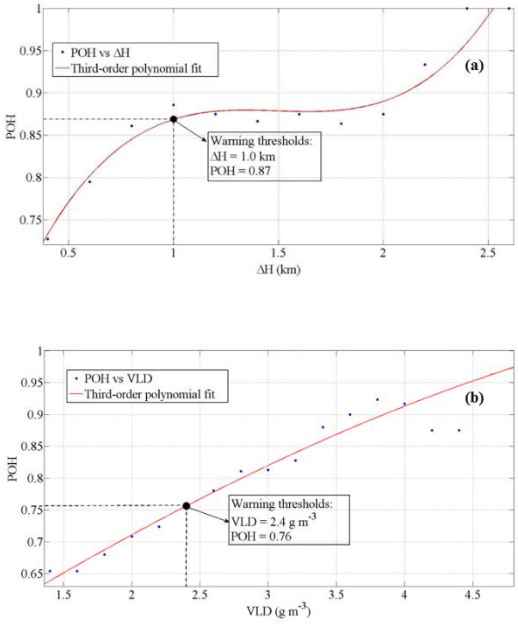

Fig. 8. The Probability of Hail (POH) as a function of ΔH (a) and VLD (b). The POH indexes, shown as red curves, have been obtained through an empirical approach, using a third-order polynomial fit. The warning thresholds (i.e. the threshold above which hail is occurring) are indicated as black filled circle over both panels.

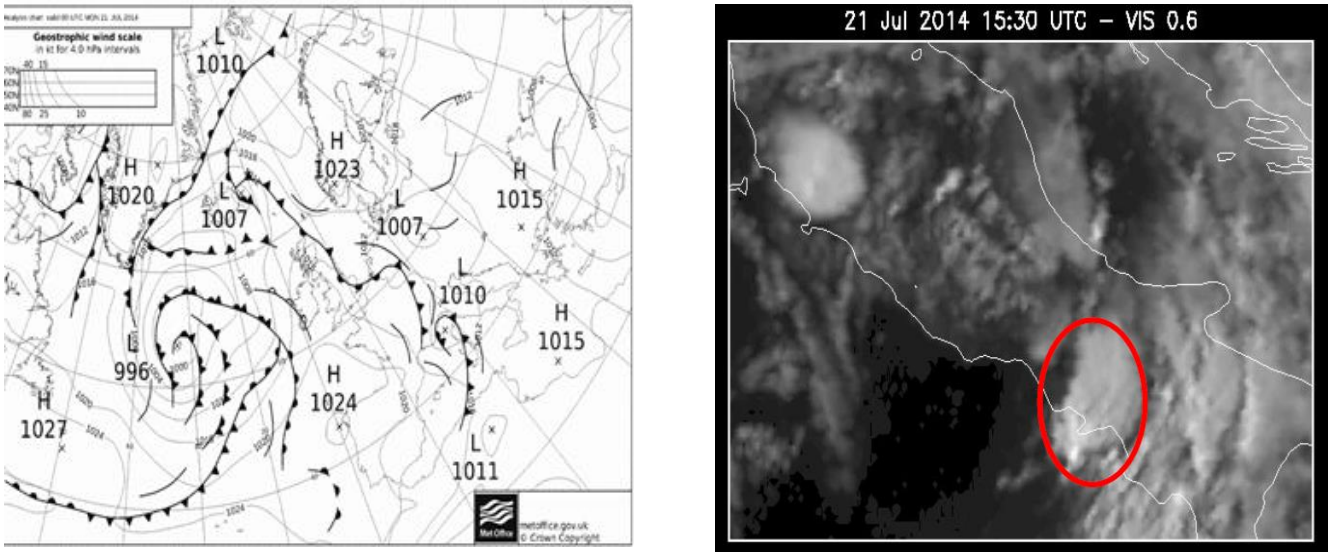

Fig. 9. In the left panel, surface pressure and weather fronts on 21 July 2014 (00:00 UTC) are shown. In the right panel, a Meteosat Second Generation visible (0.6 μm) image (collected at 15:30 UTC) is shown. The thunderstorm that caused hail precipitation in Sorrentine peninsula (highlighted by the red circle) exhibited a V-shaped pattern.

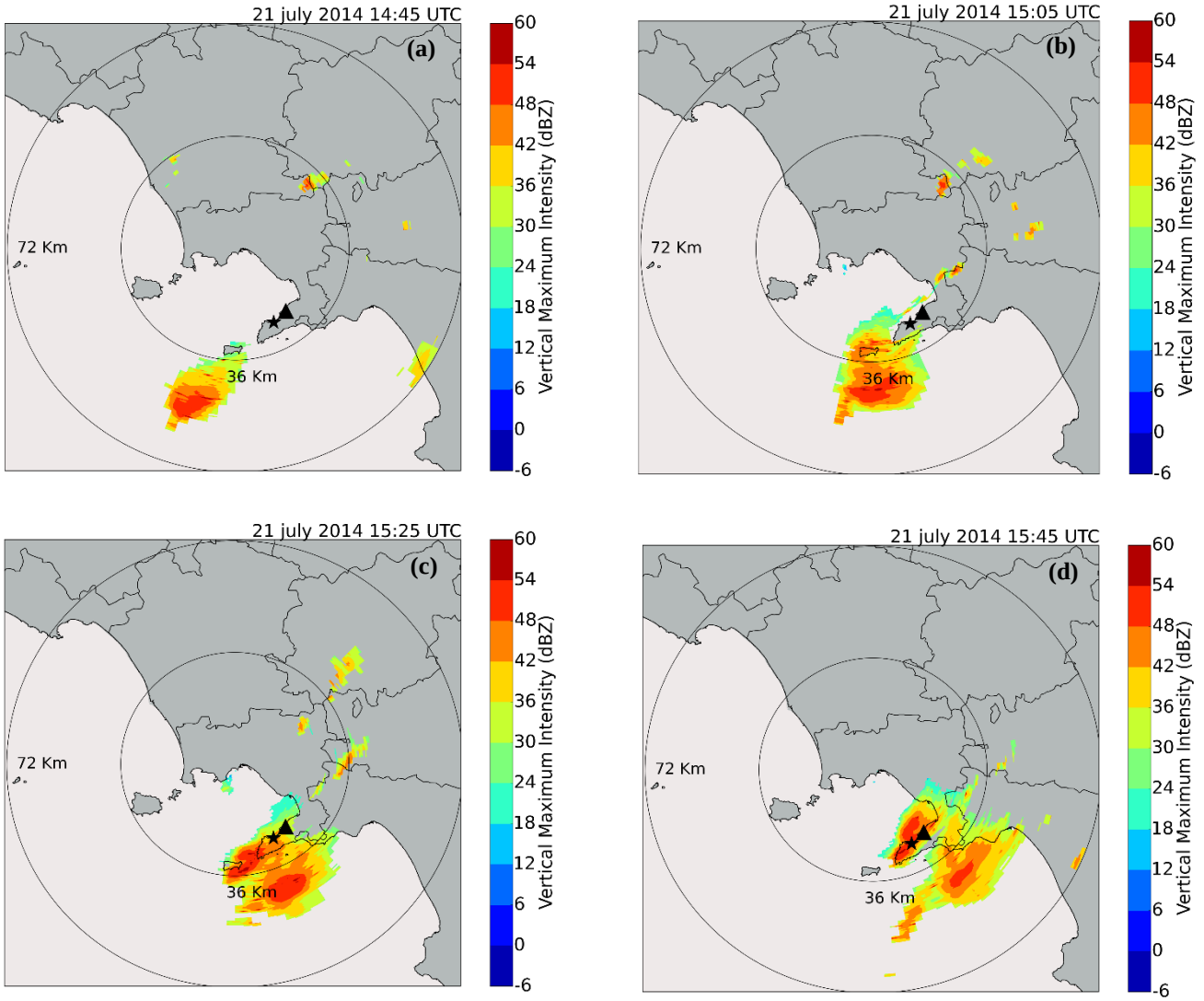

Fig. 10. WR-10X images showing the evolution of hailstorm that affected the city of Sorrento on 21 July 2014. Vertically Maximum Intensity (VMI) product obtained at 14:45 UTC (a), 15:05 UTC (b), 15:25 UTC (c) and 15:45 (d) is shown. The thunderstorm cell developed over Tyrrhenian sea and then moved from south-western to north-eastern, affecting both the Gulf of Naples and the Gulf of Salerno. The black star marker highlights the location of Sorrento city, while the black triangle marker the location of Vico Equense city.

Fig. 11. Two photografic evidences of hailstones produced by convective cell that affected the city of Sorrento on 21 July 2014.

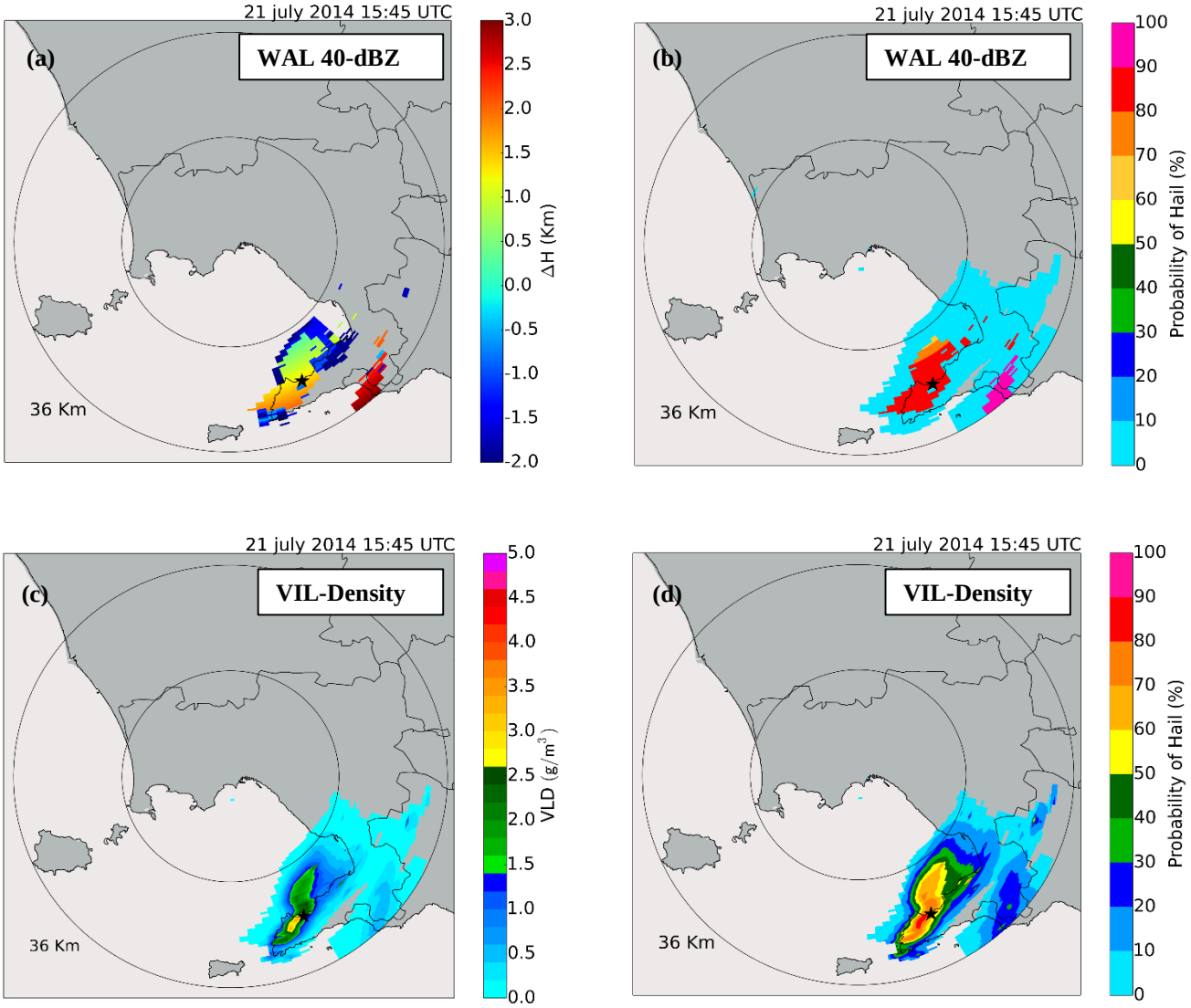

Fig. 12. Hail detection products and Probability of Hail indexes obtained by WR-10X when the hailstorm passed over Sorrento city (highlighted by black star). In the left panels, the ΔH map from WAL 40-dBZ criterion (a) and the VLD map from VIL-Density criterion (c) are shown. In (b) and (d), the related POH maps for the hail event occurred on 21 July 2014 (15:45 UTC) are presented. To better display the thunderstorm core features in the area of interest, a zoom on the Gulf of Naples has been performed.